# Carboxylic Acid-Doped SBA-15 Silica as a Host for Metallo-supramolecular Coordination Polymers†

**D. Akcakayiran,‡ D. Mauder,§ C. Hess,||,⊥ T. K. Sievers,# D. G. Kurth,# I. Shenderovich,§ H.-H. Limbach,§ and G. H. Findenegg*,‡**

*Institut für Chemie, Technische Universität Berlin, Strasse des 17. Juni 124, D-10623 Berlin, Germany, Institut für Chemie and Biochemie, Freie Universität Berlin, Takustrasse 3, D-14195 Berlin, Germany, Fritz-Haber-Institut der Max Planck Gesellschaft, D-14195 Berlin, Germany, and Max-Planck-Institut für Kolloid- and Grenzflächenforschung, D-14424 Potsdam, Germany*

*Received: May 28, 2008; Revised Manuscript Received: August 8, 2008*

The adsorption of a metallo-supramolecular coordination polymer (Fe−MEPE) in the cylindrical pores of SBA-15 silica with pure and carboxylic acid (CA) carrying pore walls has been studied. Fe−MEPE is an intrinsically stiff polycation formed by complexation of Fe(II)−acetate with an uncharged ditopic bis-terpyridine ligand. The adsorption affinity and kinetics of the Fe−MEPE chains is strongly enhanced when the pore walls are doped with CA, and when the pH of the aqueous medium or temperature is increased. The initial fast uptake is connected with a decrease of pH of the aqueous solution, indicating an ion-exchange mechanism. It is followed by a slower (presumably diffusion-controlled) further uptake. The maximum adsorbed amount of Fe−MEPE in the CA-doped material corresponds to a monolayer of Fe−MEPE chains disposed side-by-side along the pore walls. The stoichiometry of Fe−MEPE in the pores (determined by XPS) was found to be independent of the loading and similar to that of the starting material. The mean chain length of Fe−MEPE before and after embedding in the CA-doped matrix was studied by solid-state $^{15}$N NMR using partially $^{15}$N-labeled Fe−MEPE. It is shown that the average chain length of Fe−MEPE is reduced when the complex is incorporated in the pores.

## 1. Introduction

A new era in inclusion chemistry began with the discovery of periodic mesoporous materials such as SBA-15 silica,[1] which constitutes a 2D-hexagonal arrangement of cylindrical pores with diameters in a range of 6−12 nm. Because of their wide pore openings and narrow pore size distribution and their large internal surface area, these materials have a high potential as catalyst supports[2,3] and host materials for organic guest molecules. Incorporation of functional molecular components or metal ions into such a mesoporous oxide matrix can be carried out in different ways, by a one-pot synthesis,[4] ion-exchange,[5−7] covalent grafting followed by ion exchange,[8] solid-state grinding,[9] or direct loading by sorption.[10,11] Among the incorporated functional molecular components, dyes and related molecules represent an important class. For instance, Fe−MEPE,[10] methylene blue, rhodamin 6G, thionine dyes,[12] coumarine derivate dyes,[13] fluorescein,[14] direct blue 71 dye,[15,16] and chromophores[17] have been incorporated into mesoporous silica matrices. In many cases, the interaction between the dye molecules and the host system causes a shift of UV−vis absorption bands. Because of this interaction with the host, a higher degree of organization and increased diffusion stability of the guest can be achieved, which is of importance for potential applications in lasers, optical sensors, photochromic materials, or photocatalysts.[15,17,18]

In continuation of our earlier work,[10] we report here new results on the uptake of a metallo-supramolecular coordination polyelectrolyte (MEPE) in SBA-15-type silica matrices. MEPE materials are prepared by a metal ion-induced self-assembly of two-valent transition metal ions with ditopic terpyridine ligands. The resulting materials exhibit several potentially useful properties such as electro-chromic behavior,[19−21] molecular magnetism,[22] as well as dynamic properties due to the labile metal ion ligand interaction.[23] The properties of MEPE are readily manipulated by simply changing the ligands or metal ions. The substance studied in this work, Fe−MEPE (**2**) (see Scheme 1a), is assembled from Fe(II)−acetate and 1,4-bis-(2,2′:6′2″-terpyridine-4′-yl) benzene (**1**), which results in a stereochemically well-defined octahedral coordination geometry with $D_{2d}$ symmetry.[24] Accordingly, Fe−MEPE has a linear rigid-rod-like structure (ca. 1.2 nm diameter), in which the Fe(II) ions are positioned at a distance of 1.55 nm. At an exact 1:1 stoichiometry of metal to ligand, the average length of the Fe−MEPE chains in aqueous solution can grow to very high values, depending on concentration, temperature, and pH. Small deviations from 1:1 stoichiometry are causing a reduction of chain length.[23] Hence, the metal-to-ligand stoichiometry is another important parameter affecting the properties of the resulting assemblies and the amount of MEPE adsorbed in the pores.

A prominent feature of Fe−MEPE is the positive charge along the backbone. This implies that screened electrostatics plays an important role in the interaction of MEPE with the silica pore wall, which at ambient pH is negatively charged due to the weakly acidic surface silanol groups. It is of interest to see

† Part of the "Janos H. Fendler Memorial Issue".

* Corresponding author. Phone: +49 30 314 24171. E-mail: findenegg@chem.tu-berlin.de.

‡ Technische Universität Berlin.

§ Freie Universität Berlin.

|| Fritz-Haber-Institut der Max Planck Gesellschaft.

⊥ Present address: Eduard-Zintl-Institut für Anorganische and Physikalische Chemie, Technische Universität Darmstadt, Petersenstrasse 20, D-64287 Darmstadt, Germany.

# Max-Planck-Institut für Kolloid- and Grenzflächenforschung.

10.1021/jp804712w CCC: $40.75 
Published on Web 10/08/2008

**SCHEME 1: (a) Metallo-supramolecular Coordination Polyelectrolyte (MEPE) Formed by Self-Assembly of Fe(II) Ions with the Ditopic Ligand 1,4-Bis-(2,2′:6′2″-terpyridine-4′-yl)-benzene (1); (b) Monotopic Complex Fe−Terpy (4) Formed by Complexation of Fe(II) Ions and 2,2′:6′2″-Terpyridine (3); and (c) Cartoon of the Cylindrical Mesopores of SBA-15 and CA−SBA-15, in Which the Pore Walls Are Decorated by Propionic Acid Groups, Indicated Here by −COOH**

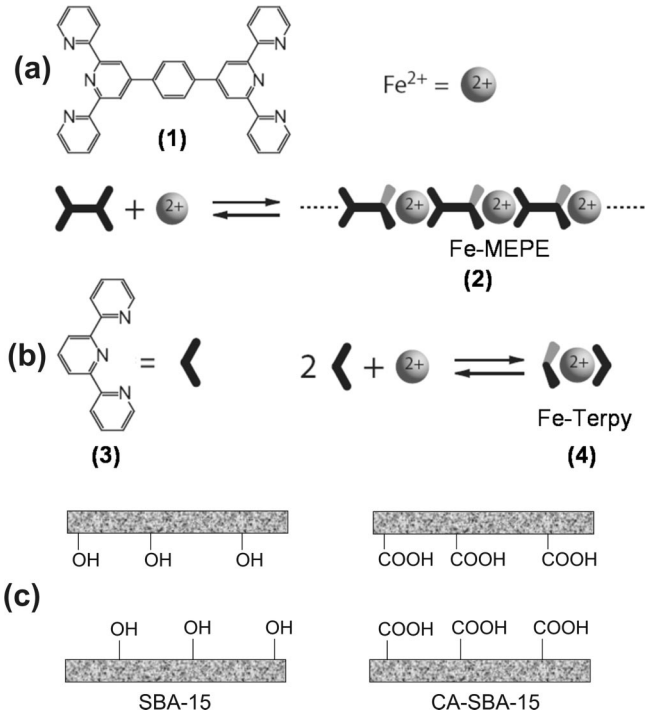


if this charge effect can be boosted by decorating the pore walls with acidic groups. For this purpose, a chemically modified SBA-15 material with short-chain carboxylic acid groups grafted to the pore walls (CA−SBA-15) was prepared (see Scheme 1c). The carboxylic acid (CA) functionality was chosen because the ionized form of these groups is similar to the acetate ions, which form the counterions of MEPE in solution. The transfer of the MEPE polycations from solution into the pores may represent an ion exchange process, involving either the ionization of carboxylic acid groups at the pore wall and a release of protons or the release of the counterions of MEPE polycations. In either case, the ion exchange represents an entropic driving force for the adsorption of MEPE in the pores. To test this possible mechanism, we made a comparative study of the uptake of Fe−MEPE in pure ("native") SBA-15 and CA-doped SBA-15 materials. We also studied the effect of temperature and pH on the uptake of MEPE, as both can affect the sorption process.

Another interesting question concerns the mechanism of the MEPE uptake and the mean chain length of MEPE in the pores. It is known that in aqueous media, due to the labile nature of the metal ion ligand interaction, MEPE represent dynamic equilibrium polymers; that is, assemblies of different length coexist in solution.[25] It is feasible that short chains adsorb more easily into the pores or that longer chains break into shorter chain segments when entering the pore. These processes would lead to a shorter chain length of MEPE in the pores as compared to the solution. Alternatively, short chain segments may merge into longer ones in the pores if the pore walls stabilize the chains. Two ways for studying the chain length of MEPE in the pores are used in this work: (I) Indirect information is derived from the number ratio of metal ions to carbon or nitrogen atoms in the pore, which can be determined by X-ray photoelectron spectroscopy (XPS). (II) A more direct way is to measure the ratio of terminal and internal terpyridine groups of the Fe−MEPE using solid-state NMR spectroscopy. This latter method requires $^{15}N$ NMR measurements, which made it necessary to synthesize a $^{15}N$-labeled ligand.

A combination of experimental techniques was used to characterize pure and CA-doped SBA-15 materials and the state of Fe−MEPE in the pores. The silica samples before MEPE incorporation were characterized by nitrogen adsorption, small-angle X-ray diffraction (SAXD), and solid-state $^{29}Si$ and $^{13}C$ NMR, whereas Fe−Terpy and Fe−MEPE in solution and incorporated in the silica materials were studied by UV−vis spectroscopy, atomic absorption spectroscopy (AAS), X-ray photoelectron spectroscopy (XPS), and $^{15}N$ solid-state NMR. The materials and methods used in this study are briefly introduced in section 2, and the results are presented in section 3. The Discussion (section 4) is focused on the driving forces for the uptake of MEPE in the pores, the maximum uptake, and the stoichiometry and average chain length of Fe−MEPE in the pores of pure and CA-doped SBA-15. Finally, section 5 winds up the main findings of the work.

## 2. Experimental Section

**2.1. Materials.** ***Pure SBA-15.*** SBA-15 was prepared by the method reported in ref 1 using tetraethoxysilane (TEOS, 99%, ABCR) as the silica precursor and technical-grade poly(ethylene oxide)−poly(propylene oxide)−poly(ethylene oxide) triblock copolymer (Pluronic P123, BASF USA, Mount Olive, NJ) as the structure-directing agent. The molar composition of the reaction mixture was 1TEOS:5.9$H_2SO_4$:323$H_2O$:0.017P123. The polymer−silica composite, formed as a fine precipitate, was kept in the reaction solution at 40 °C for 5 h under constant stirring and then transferred to an autoclave for aging (20 h at 105 °C). The product was filtered, washed with milli-Q water, dried at 60 °C, and finally calcined in air at 550 °C.

***Carboxylic Acid-Doped SBA-15 (CA−SBA-15).*** Materials were prepared by a one-pot synthesis reported in ref 26. The functional silane 2-cyanoethyl triethoxysilane (CTES, 98%, Aldrich) was added to a hydrochloric acid solution of P123 at 40 °C, and the solution was stirred for 1 h. Silica precursor TEOS was added, and the mixture was stirred for 20 h, followed by aging at 90 °C without stirring. The molar composition of the system was $(1 - x)$TEOS:$x$(CTES):5.8HCl:193$H_2O$:0.017P123, where $x = 0.1$ and 0.2. The as-synthesized products were filtered, washed, and dried at 80 °C. To remove the template and to hydrolyze the −CN groups, 1 g aliquots of the material were suspended in 150 mL of 48% $H_2SO_4$ and stirred at 95 °C for 24 h. The resulting propionic acid-doped product was washed extensively, first with acetone and ethanol and later with water until the pH of the eluent was pH neutral, and finally dried at 60 °C. To promote template removal, 10-CA was calcined at 250 °C for 2.5 h. The products with $x = 0.1$ and $x = 0.2$ are called 10-CA and 20-CA, respectively, where the numbers 10 and 20 give the mole percent of CTES in the silica precursor mixture.

***Fe−MEPE (MEPE).*** The ligand 1,4-bis-(2,2′:6′2″-terpyridine-4′-yl)-benzene and Fe−MEPE (see Scheme 1a) were synthesized as described elsewhere.[27−29] Terephthaldialdehyde, acetylpyridine, ammonia solution (25%), and ethanol were purchased from Sigma-Aldrich and used without further purification. Throughout this work, Fe−MEPE was used in the form

of the acetate salt. The assembly of ligand **1** and $Fe(OAc)_2$ (Sigma-Aldrich, 99.995%) was carried out in 75% acetic acid. In view of the oxidation sensitivity of $Fe(OAc)_2$ after contact with air, the Fe−MEPE material used in most of this work (material I) was prepared with a small excess of the iron salt. The $^{15}N$ NMR measurements aimed at determining the average chain length of Fe−MEPE before and after uptake in the pores were performed with a Fe−MEPE sample (material II) assembled under inert conditions from freshly prepared $Fe(OAc)_2$ and $^{15}N$-labeled ligand at an initial metal-to-ligand stoichiometry of 0.8:1. Complementary $^{15}N$ NMR measurements to characterize the Fe−MEPE in the solid state were made with two unlabeled Fe−MEPE samples (material III and material IV) of 1:1 and 0.8:1 metal-to-ligand stoichiometry, respectively.

***Fe−Terpy.*** The ligand 2,2′:6′2″-terpyridine (Terpy (**3**), see Scheme 1b) was purchased from Sigma-Aldrich (98%) and used without further purification. Fe−Terpy, $Fe(Terpy)_2(OAc)_2$, was prepared according to standard procedures published by Margan and Burstall using freshly prepared $Fe(OAc)_2$ and Terpy in 75% acetic acid.[30]

Both Fe−MEPE and Fe−Terpy show intense absorption bands in the UV−vis spectrum between 270 and 320 nm resulting from $\pi \rightarrow \pi^*$ transitions, and weaker bands at 370 and 360 nm due to d→d transitions. The bands at 586 and 552 nm are related to a metal-to-ligand charge transfer (MLCT) transition, which is characteristic for octahedrally coordinated Fe(II)−bis-terpyridine complexes.[31]

**2.2. Methods.** The pore structure of silica materials was characterized by $N_2$ adsorption and small-angle X-ray diffraction. Adsorption isotherms were measured by gas volumetry using a Gemini 2375 apparatus by Micromeritics. Small-angle X-ray diffraction (SAXD) profiles were recorded in a range of the scattering vector $q$ from 0.3 to 2 $nm^{-1}$ by a Bruker SAXS Nanostar machine using the 2D HI Star area detector and Cu Kα radiation ($\lambda$ = 1.54 Å). XPS measurements were carried out using a modified LHS/SPECS EA200 MCD system equipped with a Mg Kα source (1253.6 eV, 168 W). The binding energy scale of the system was calibrated using $Au4f_{7/2}$ = 84.0 eV and $Cu2p_{3/2}$ = 932.67 eV from foil samples. The powder samples were placed in a stainless steel sample holder with a 0.6 mm deep rectangular well, covering an area of (12 × 8) $mm^2$. During the XPS experiments, the pressure in the UHV analysis chamber increased to about $1 \times 10^{-9}$ mbar. The binding energies of the SBA-15-based samples were referenced to the Si2p signal of silica at 103.6 eV to correct for charging.[32] Data reduction included satellite deconvolution and subtraction of a Shirley background. Quantitative data analysis was performed on the basis of peak areas by fitting with 30/70 Gauss−Lorentz product functions. Atomic ratios were calculated using empirical cross sections.[33] Atomic absorption spectroscopy (AAS) measurements of Fe in the silica matrix were made by a 1100B Perkin-Elmer Flame AAS spectrometer after dissolving the silica matrix in 25 mL of 0.1 M NaOH. To dissolve the Fe−MEPE which precipitates in this high pH region, 2 mL of each sample solution was acidified with concentrated HCl and filled to 10 mL with milli-Q water. After this pretreatment, the flame atomization was performed in an air−acetylene gas mixture. Calibration was made with 0.1 M $FeCl_3$ standard (titrisol) by means of the standard addition method. UV−vis absorption spectra were recorded on a Carry 50 UV−vis spectrometer by Varian using quartz glass cells of 1 mm thickness.

***NMR Measurements.*** NMR measurements were performed on a Bruker MSL-300 instrument operating at 7 T, equipped with a Chemagnetics-Varian 6 mm pencil CPMAS probe. Samples were spun at 6.0 kHz ($^{13}C$ and $^{29}Si$ NMR) or 6−8 kHz ($^{15}N$ NMR) under magic angle spinning (MAS) conditions. The $^{29}Si$ MAS spectra were recorded employing a $\pi/12$ pulse-sequence, a recycle delay of 180 s, and 800 scans. The $\{^1H\}-^{29}Si$ CPMAS spectra were recorded using a relatively long cross polarization (CP) contact time of 8 ms to ensure sufficient polarization transfer to all different species of silica, that is, $Q^2$, $Q^3$, and $Q^4$; further parameters were a recycle delay of 5 s and 2000 scans. The $^{13}C$ NMR measurements were performed employing the $\{^1H\}-^{13}C$ CPMAS technique with a CP contact time of 2 ms and a recycle delay of 5 s. The typical 90° pulse length in the CP experiments was 3.5 μs for $^1H$. The $^{13}C$ and $^{29}Si$ chemical shift values are referenced to solid TSP. $^{13}C$ and $^{29}Si$ NMR spectra of the carboxylic acid-doped materials are shown in section S1 of the Supporting Information.

The $^{15}N$ MAS spectra were recorded employing a $\pi/2$ pulse-sequence, with a 90°-pulse length of 4.5 μs and a recycle delay of 600 s. The $\{^1H\}-^{15}N$ CPMAS spectra were recorded using a cross polarization contact time of 5 ms; the typical 90°-pulse lengths were 3.5−4.5 μs. All $^{15}N$ chemical shift values are referenced to solid $^{15}NH_4Cl$.

***Uptake Isotherms.*** The uptake of the MEPE in the silica matrix was measured by bringing a mass $m_s$ of silica into contact with a volume $V_l$ of aqueous MEPE solution of an initial concentration $c_0$. The mass $m_t$ of the MEPE complex included in the matrix after a time $t$ was calculated from the corresponding solution concentration $c_t$ by the relation:

$$\frac{m_t}{m_s} = \frac{MV_l(c_0 - c_t)}{m_s} \tag{1}$$

where $M$ is the molar mass of the entity embedded in the pores ($M$ = 714.6 g/mol for Fe−MEPE acetate). The concentration $c_t$ was obtained from UV−vis measurements of the MLCT band of Fe−MEPE in the supernatant solution. Experiments were made at initial concentrations $c_0$ of MEPE in a range from 0.4 to 1.2 mM and different MEPE-to-silica mass ratios $\mu = m_{MEPE}/m_s$ with $m_{MEPE} = MV_lc_0$, by dissolving appropriate amounts of Fe−MEPE in the volume $V_l$ (50 mL) of milli-Q water (pH = 5.5) or 0.1 M potassium acetate solution (KOAc, pH = 7.25). For studying the time dependence of the uptake, the suspensions were slowly rotated in a test tube rotator at the chosen temperature and the concentration $c_t$ was measured after centrifugation (4000 rpm for 15 min) and taking small aliquots of the supernatant for UV−vis analysis. At the end of the uptake time, when $m_t/m_s$ had reached a steady value, the solid product, having an intense violet color, was washed two times with 50 mL of $H_2O$ and dried at 60 °C before further analysis. Blank measurements in the absence of silica indicated some settling of Fe−MEPE during centrifugation of the solution. The fraction of settled Fe−MEPE was small (less than 3%) at times up to 150 h, but became progressively more important and had to be taken into account in the calculation of the uptake at longer times. A typical blank measurement is shown in section S2 of the Supporting Information.

## 3. Results

**3.1. Characterization of Materials.** ***Pure and Carboxylic Acid-Doped SBA-15.*** The porosity of the silica materials was characterized by nitrogen adsorption. The mean pore diameter $D$ was obtained from the adsorption branch of the isotherm using the extended Kruk−Jaroniec−Sayari (ext. KJS) equation.[34] Details of the data analysis are given elsewhere.[35] SAXD profiles from pure SBA-15 and the two CA-doped silicas are displayed

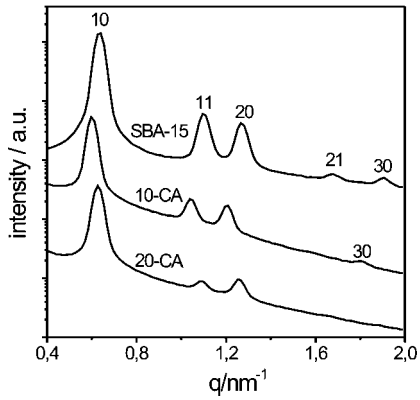


**Figure 1.** Small-angle X-ray diffraction profiles for SBA-15, 10-CA, and 20-CA. The SAXD profiles of the samples are displaced by factors of 25 for clarity.

**TABLE 1: Characterization of Pure and CA-Doped SBA-15 by Nitrogen Adsorption, SAXD, and $^{29}$Si NMR[a]**

| sample | $a_s$/m$^2$ g$^{-1}$ | $v_p$/cm$^3$ g$^{-1}$ | $D$/nm | $a_0$/nm | $x_{COOH}$ |
|---|---|---|---|---|---|
| SBA-15 | 650 | 0.89 | 8.9 | 11.50 | |
| 10-CA | 513 | 0.97 | 9.8 | 12.13 | 0.19 |
| 20-CA | 400 | 0.60 | 8.0 | 11.61 | 0.42 |

[a] BET specific surface area $a_s$, specific mesopore volume $v_p$, pore diameter $D$ (ext KJS algorithm), lattice constant $a_0 = 4\pi/(q_{10}\sqrt{3})$, and mole fraction of carboxylic groups on the surface, $x_{COOH}$.

in Figure 1. The properties derived from nitrogen adsorption and SAXD are summarized in Table 1.

The nitrogen adsorption isotherms and SAXD curves show that all of our materials are highly ordered, indicating that the 2D-hexagonal mesopore structure of SBA-15 is preserved when up to 20% of the silica precursor (TEOS) is replaced with the functional silane CTES. The lattice constant $a_0$ of the pore lattice decreases as the proportion of CTES in the silica precursor mixture is increased from 10-CA to 20-CA, and the same trend is seen in the pore diameter $D$ (Table 1). The pure SBA-15 material does not follow these trends but has smaller $a_0$ and $D$ than does 10-CA due to the shrinkage of the matrix during calcinations at 550 °C.

From the $^{13}$C CPMAS NMR spectra of 10-CA and 20-CA (shown in section S1 of the Supporting Information), it follows that all −CN groups of the functional silane are converted to −COOH, and that the block copolymer template is completely removed (or almost completely, in the case of 10-CA) by the treatment with 48 wt % $H_2SO_4$ and 2.5 h calcination at 250 °C. $^{29}$Si MAS NMR spectroscopy was used to determine relative numbers of CA groups at the pore walls of 10-CA and 20-CA. From the intensities of the $T^3$ and $T^2$ peaks (silicon atom with one organic functional groups) and of the $Q^3$ and $Q^2$ peaks (silicon atoms with one and two OH groups, respectively), the quantity $x_{COOH} = N_{COOH}/N = (T^3 + T^2)/(T^2 + T^3 + Q^2 + Q^3)$ was derived as an approximate value of the number fraction of CA groups in the mixture of −COOH and −OH groups at the pore walls. $^{29}$Si MAS NMR spectra of 10-CA and 20-CA and a table with the relative intensities of the peaks $T^3$, $T^2$, $Q^2$, and $Q^3$ are given in section S1 of the Supporting Information. The quantity $x_{COOH}$ calculated from these intensities implies that nearly 20% of the surface groups (−COOH and −OH) of 10-CA and about 40% of the surface groups of 20-CA are CA groups.

***Characterization of Coordination Compounds by NMR.*** The free terpyridine (Terpy) ligand and the Fe−Terpy complex were investigated by $^{15}$N CPMAS NMR spectroscopy to determine

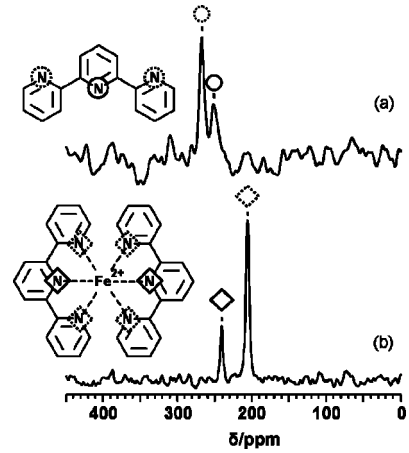


**Figure 2.** Solid-state $^{15}$N CPMAS NMR spectra of (a) free ligand Terpy and (b) $Fe(Terpy)_2OAc_2$. The signals are assigned to atoms by symbols as follows: ○, free Terpy; ◇, complexed Terpy. Solid symbols indicate N atoms of the central ring, and dashed symbols indicate N atoms of the outer rings.

the chemical shift of the different nitrogen atoms, which is needed for peak assignment of the Fe−MEPE complex. For free Terpy in its energetically preferred trans-configuration, two signals at chemical shifts of 252 ppm and 267 ppm appear, resulting from nitrogen atoms on the central ring and the outer rings, respectively (Figure 2a).

Figure 2b shows the $^{15}$N CPMAS NMR spectrum of Fe−Terpy, which is taken as a simple model of a Fe−MEPE unit. For complexation with Fe(II) ions, Terpy molecules have to change their configuration from trans to cis to allow octahedral coordination of the ligands to the center. The presence of the Fe(II) ion and the different ligand configuration have an effect on the chemical shift for the different nitrogen species in the Fe−Terpy complex. The signal at 242 ppm is assigned to the central nitrogen atom of Fe−Terpy, slightly shifted to high field, and the signal at 207 ppm is assigned to the outer nitrogen atoms of Fe−Terpy, shifted 60 ppm to high field, as compared to the free ligand.

$^{15}$N CPMAS NMR spectra of solid Fe−MEPE materials I and III, having different stoichiometric Fe:ligand ratios, are shown in Figure 3. By comparison with the $^{15}$N CPMAS NMR spectra of free Terpy and Fe−Terpy (Figure 2), we can assign each peak to either of the two types of nitrogen atoms. In the Fe−MEPE material with an Fe:ligand ratio of 1:1, only signals from Fe(II)-coordinated ligands (238 and 205 ppm) are detected (Figure 3a). This implies that nearly all ligands are coordinated to two Fe(II) ions, so that the number of noncoordinated nitrogen atoms at the chain ends is too small to be detected by solid-state $^{15}$N NMR. From this, we conclude that Fe−MEPE with an Fe:ligand ratio of 1:1 consists of long chains. However, as such long chains are hardly soluble in aqueous media, they are unsuitable for uptake studies into the porous matrix. Accordingly, a Fe−MEPE sample with an Fe:ligand stoichiometry of approximately 0.8: 1 (material IV) was used because an excess of ligand results in shorter Fe−MEPE chains.[23] The $^{15}$N NMR spectrum of this Fe−MEPE sample (Figure 3b) shows two additional signals corresponding to N atoms in free ligands at chain ends (269 and 259 ppm) besides the signals from coordinated ligands (242 and 206 ppm). This result illustrates that $^{15}$N solid-state NMR can be used to estimate the chain length of Fe−MEPE by analyzing the signal intensities of coordinated and free N atoms of the ligand. An estimate of the mean chain length of Fe−MEPE before and after inclusion into

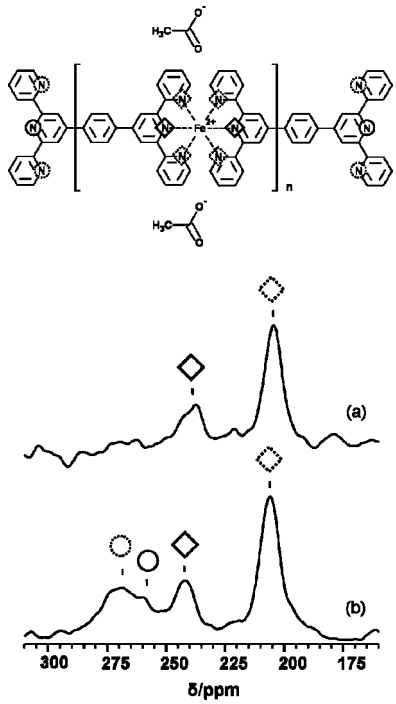


**Figure 3.** Solid-state $^{15}N$ CPMAS NMR spectra of (a) Fe−MEPE material III with an Fe:ligand ratio of 1:1; (b) Fe−MEPE material IV with an Fe:ligand ratio of 0.8:1. Fe−MEPE chains of 1:1 stoichiometry (spectrum a) are long, and thus no end groups are detected. In the material having a ligand excess (spectrum b), uncoordinated N atoms are present at an appreciable concentration.

the pores by signal deconvolution of the respective signals is presented in section 3.4.

**3.2. Effect of CA-Doping on the Fe−MEPE Uptake.** The uptake of Fe−MEPE (material I) in the silica matrix as a function of time was determined by UV−vis spectroscopy as explained in the Experimental Section. The strong MLCT band is ideally suited to quantify the concentration of Fe−MEPE. The uptake of Fe−MEPE into the cylindrical pores of pure and CA-doped SBA-15 was studied at different mass ratios of Fe−MEPE and silica matrix $\mu$ in a range from 0.05 to 0.3.

Figure 4 shows a typical example for the decreasing intensity of the MLCT band in the supernatant solution as a function of time (a), and the respective uptake isotherms (b) for Fe−MEPE in pure SBA-15 and 20-CA. For both samples, we observe a fast initial uptake of Fe−MEPE. This fast process is most pronounced for 20-CA: At a MEPE-to-silica mass ratio $\mu$ = 0.05, it leads to nearly complete uptake within 2 h, indicated by a change of the initially deep blue color of the Fe−MEPE solution to completely colorless, while the initially colorless silica turned violet. For pure SBA-15 at the same MEPE-to-silica mass ratio, the fast process leads to a lower uptake, but is followed by a much slower second uptake process that leads to nearly complete uptake after about 600 h. This slow process also takes place with Fe−MEPE in 20-CA at a higher MEPE-to-silica mass ratio ($\mu$ = 0.10), where it leads to an increase in the MEPE uptake from 50% to more than 80% of the overall amount after about 200 h (Figure 4b).

It is well-known that SBA-15 materials with carboxylate groups have cation-exchange properties.[36] To check whether ion exchange is a driving force in the uptake of Fe−MEPE in the present materials, time-dependent measurements of pH were performed with freshly prepared suspensions of the silica materials in aqueous Fe−MEPE solutions in the absence of KOAc. Results for 10-CA and pure SBA-15, both

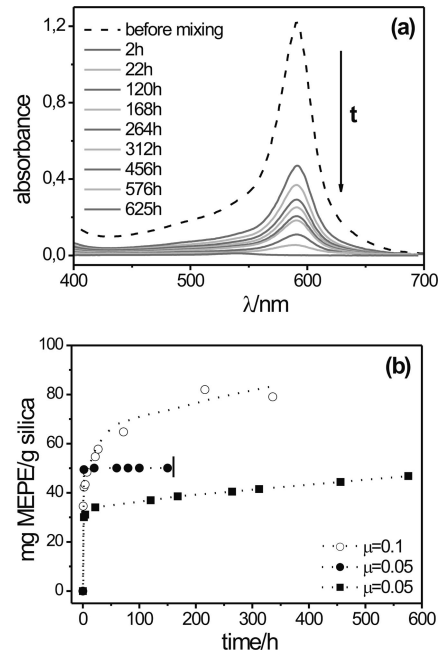


**Figure 4.** Example of the uptake of Fe−MEPE from 0.1 M KOAc into pure SBA-15 and the CA-doped material 20-CA: (a) Decrease of the MLCT band of the supernatant solution during an uptake experiment with pure SBA-15; (b) corresponding uptake isotherms into pure SBA-15 (■) and 20-CA (●) at a MEPE/silica mass ratio $\mu$ = 0.05, and into 20-CA at $\mu$ = 0.1 (○). Curves are drawn to guide the eye.

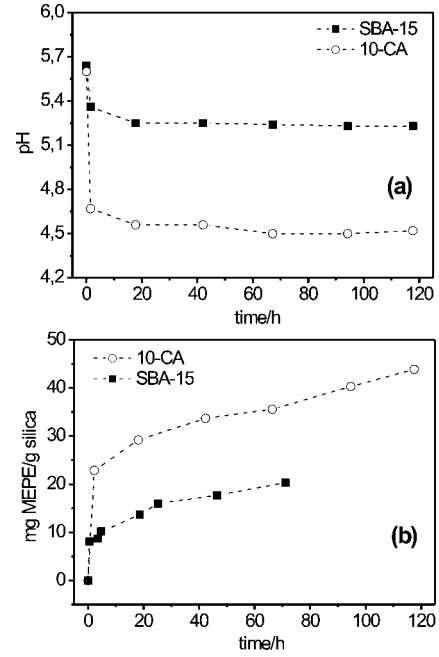


**Figure 5.** Uptake of Fe−MEPE in pure SBA-15 and 10-CA (20 °C): (a) Evolution of pH in the aqueous solution before ($t$ = 0) and after addition of the silica ($t$ > 0); (b) uptake isotherms in the two materials (MEPE-to-silica mass ratio $\mu$ = 0.10, room temperature). Dashed curves are drawn as a guide to the eye.

at $\mu$ = 0.10, are displayed in Figure 5a, and the respective uptake isotherms are shown in Figure 5b. The initial pH (5.6) represents the value of the MEPE solution in milli-Q water. Addition of the silica causes a decrease in pH, from 5.6 to 5.2 for pure SBA-15 and from 5.6 to 4.5 for 10-CA, during the first 1.5−2 h, that is, in the period of the fast uptake process. Later, during the slow uptake process, the pH of the suspensions remains constant. The finding that the pH

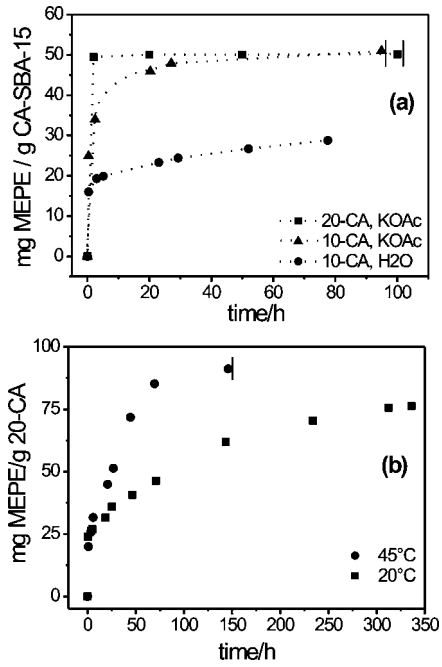


**Figure 6.** Effect of pH and temperature on the uptake isotherms of Fe−MEPE in carboxylic acid-doped SBA-15: (a) 10-CA at pH 5.5 (●); 10-CA at pH 7.3 (▲); 20-CA at pH 7.3 (■); (b) effect of temperature on the uptake rate in 20-CA ($\mu = 0.1$) without added salt. The vertical bars indicate complete uptake; dashed lines are drawn as a guide to the eye.

change is linked with the fast uptake process of MEPE indicates that ion exchange is indeed involved in this step. Moreover, the larger pH change induced by 10-CA, as compared to the pure SBA-15, is in line with the larger initial uptake of MEPE in 10-CA (Figure 5b).

To assess the influence of pH, and thus the degree of dissociation of the CA groups at the pore wall, a comparison of the uptake of Fe−MEPE from pure water (initial pH 5.5) and from 0.1 M KOAc solution (pH 7.3) was made. Uptake isotherms for MEPE at an initial concentration $c_0 = 0.4$ mM and a MEPE-to-silica mass ratio $\mu = 0.05$ are shown in Figure 6a. It can be seen that in 10-CA both the fast and the slow uptake processes are more effective at the higher pH, at which complete uptake is accomplished within about 50 h. At the lower pH, at which one expects a lower degree of ionization of the CA groups at the pore wall, the fast process leads to a lower initial uptake, and the slow process proceeds at a significantly lower rate than at higher pH. Figure 6a also indicates that at a given pH (7.3) the uptake of MEPE in 10-CA is less effective than that in 20-CA, for which complete uptake is accomplished within 2 h at the given MEPE-to-silica mass ratio.

We also studied the effect of temperature on the rate of uptake of Fe−MEPE into the pores of pure and CA-doped SBA-15. Results for Fe−MEPE in 20-CA at 20 and 45 °C are shown in Figure 6b. In this example ($\mu = 0.09$) at 45 °C, nearly complete uptake was reached after 150 h, while at 20 °C uptake was not complete after 350 h. This behavior indicates a significant kinetic resistance for the slow process. For this reason, measurements of the equilibrium adsorption isotherm were performed at an elevated temperature. Figure 7 shows data for the uptake of Fe−MEPE in 20-CA up to 300 h as a function of the concentration in the supernatant solution. The individual data points correspond to different initial MEPE-to-silica ratios $\mu$. Also shown in this figure are two points for the adsorption of Fe−MEPE in pure SBA-15, to indicate the large difference in

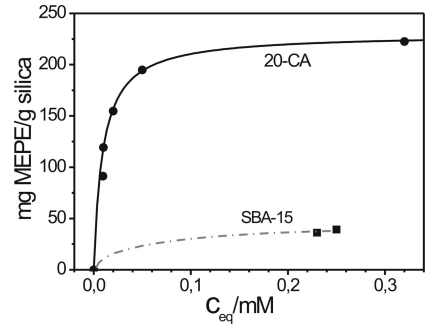


**Figure 7.** Adsorption isotherms of Fe−MEPE from aqueous solution (without added salt) in 20-CA (■); pure SBA-15 (●); results for different MEPE-to-silica ratios $\mu$ at 50 °C. The solid line represents a fit of the 20-CA data by the Langmuir equation; the dashed−dotted line for the data in SBA-15 is drawn to guide the eye.

**TABLE 2: Fe−MEPE (Material I) in SBA-15 (SBA−MEPE) and in 20-CA (CA−MEPE-4−8) Prepared for Comparative Studies[a]**

| sample | $c_0$/mM | $\mu$ | $m_{Fe-MEPE}/m_{SiO2}$ | $S$ |
|---|---|---|---|---|
| SBA−MEPE | 0.37 | 0.094 | 0.033 | 3 |
| CA−MEPE-4 | 0.37 | 0.094 | 0.091 | 10 |
| CA−MEPE-5 | 0.48 | 0.122 | 0.119 | 13 |
| CA−MEPE-6 | 0.62 | 0.159 | 0.156 | 17 |
| CA−MEPE-7 | 0.81 | 0.207 | 0.195 | 21 |
| CA−MEPE-8 | 1.20 | 0.305 | 0.223 | 24 |
| CA−$^{15}$N-MEPE[b] | 1.27 | 0.225 | 0.219 | 18 |

[a] $c_0$, initial MEPE concentration; $\mu$, MEPE-to-silica mass ratio; $m_{Fe-MEPE}/m_{SiO2}$, specific uptake of Fe−MEPE acetate; $S$, number of MEPE chains accommodated side-by-side in the pores. [b] CA−$^{15}$N-MEPE is prepared from a different 20-CA charge using Fe−MEPE material II.

adsorption affinity between pure and carboxylic acid-doped SBA-15. A detailed account of the adsorption kinetics of Fe−MEPE in 20-CA will be presented elsewhere.[37]

**3.3. Characterization of Fe−MEPE in CA−SBA-15.** To characterize the state of Fe−MEPE in the pores of pure and CA-doped SBA-15 materials, some of the composite samples were studied by a combination of different techniques. The effect of MEPE uptake on the properties of the matrix was determined by nitrogen adsorption and SAXD measurements, while the Fe−MEPE content was determined by atomic absorption spectroscopy (AAS) and X-ray photoelectron spectroscopy (XPS). Composite samples were prepared by exposing the silica to Fe−MEPE solutions (50 mL) of different initial concentrations $c_0$ and different MEPE-to-silica mass ratios $\mu$, and centrifugation after 300 h. (The terms bare silica and composite sample are used for the silica samples without and with embedded Fe−MEPE, respectively.) Table 2 gives the Fe−MEPE content of these samples, expressed as adsorbed mass of Fe−MEPE per unit mass of silica, and as the mean number of MEPE chains accommodated side-by-side in a pore. Both quantities were derived from the UV−vis depletion measurements. The samples specified as CA−MEPE-4 to CA−MEPE-6 come from the high-affinity regime of the MEPE uptake by the silica. The samples CA−MEPE-7, CA−MEPE-8, and CA−$^{15}$N-MEPE result from the highest initial MEPE concentrations $c_0$ and highest MEPE-to-silica mass ratios $\mu$, at which the uptake was not complete after 300 h. Values of the Fe−MEPE content of these samples were corrected for the effect of sedimentation of Fe−MEPE during the centrifugation step (see section S2 of the Supporting Information).

A comparison of nitrogen adsorption isotherms and SAXD profiles of the CA-doped samples and the respective bare silicas

indicated that the pore structure of the CA-doped silicas was not significantly affected but that the pore volume can be changed by the long-term exposure to the aqueous MEPE solutions at ambient or elevated temperatures. We attempted to quantify this effect by reference measurements in which the bare 20-CA material was exposed to the aqueous medium. On this basis, the volume occupied by the embedded Fe−MEPE in the pores was estimated from the nitrogen adsorption isotherms. It was found that this volume is consistent with the amount of embedded Fe−MEPE determined by UV−vis measurements. This is explained in section S3 of the Supporting Information, where nitrogen adsorption isotherms and SAXD profiles for some of the samples are presented.

The samples CA−MEPE-4, CA−MEPE-6, and CA−MEPE-8 were characterized by taking XPS spectra of carbon, nitrogen, and iron. Figure 8A shows C1s XPS spectra of bare 20-CA (a) and of the samples CA−MEPE-4 (b) and CA−MEPE-6 (c). The peaks at 285.1 and 289.6 eV of bare 20-CA are assigned to the carbon atoms of the alkyl and carboxyl groups, respectively, of the propionic acid groups at the pore wall. Upon loading with Fe−MEPE, a shift of the 285.1 eV peak to 285.4 eV is observed. To compare the spectral features of embedded Fe−MEPE with bulk Fe−MEPE, difference spectra were calculated by subtraction of spectrum (a) from spectra (b) and (c). The resulting difference spectra are displayed in Figure 8B as spectra (a) and (b). Regarding the peak position of the signal at 285.4 eV, the C1s spectra of embedded Fe−MEPE closely resemble the respective spectrum of bulk Fe−MEPE, which is shown as spectrum (c) in Figure 8B. The observed binding energy of 285.4 eV is in good agreement with the literature value of 285.5 eV for pyridine.[38] Figure 8B also shows that the intensity of the C1s signal of the embedded Fe−MEPE increases from CA−MEPE-4 to CA−MEPE-6.

Figure 8C shows X-ray photoelectron Fe2p$_{3/2}$ spectra of Fe−MEPE in the samples CA−MEPE-4 (a) and CA−MEPE-6 (b); the respective Fe2p$_{3/2}$ spectrum of bulk Fe−MEPE normalized in intensity to spectrum (b) is shown as spectrum (c). All spectra are characterized by an asymmetric peak with an intensity maximum at 709.3 eV. This value of the binding energy as well as the shape of the asymmetric tail are consistent with results reported for other Fe(II) compounds such as Fe(phthalocyanine)[39] or FeO.[40] However, due to the complexity of the X-ray photoelectron Fe2p spectra, a contribution of Fe(III) ions cannot be ruled out.

X-ray photoelectron N1s spectra of the samples CA−MEPE-4 and CA−MEPE-6 and bulk Fe−MEPE were also determined. From the normalized intensities of the N1s and Fe2p$_{3/2}$ signals, the atom ratio N/Fe of the MEPE complexes in the pores was determined (Table 3).

Table 3 compares the iron content of the 20-CA−MEPE composite samples as determined by three methods, depletion of the supernatant solution (UV−vis), AAS, and XPS. The AAS and UV−vis data are in reasonably good agreement (deviation of AAS from UV−vis no greater than 12%), except for the sample with the highest loading (CA−MEPE-8) for which the AAS values are significantly lower than that obtained by the depletion method. For the sample of lowest Fe−MEPE content (CA−MEPE-4), the iron content obtained by XPS also agrees with that obtained by the depletion method. At higher loadings, however, XPS yields significantly higher values of the iron content than do the two other methods. Higher Fe concentrations obtained by XPS than by AAS may indicate higher concentrations of Fe−MEPE near the surface than in the core of the silica grains, because XPS

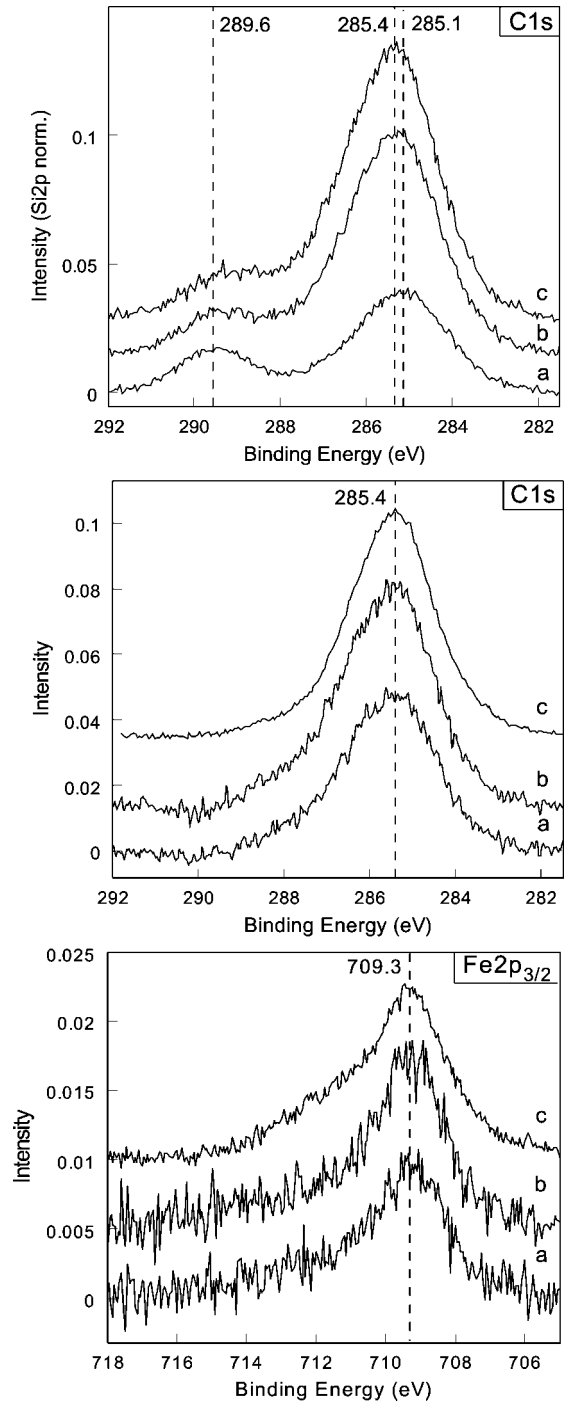


**Figure 8.** (A) Si2p normalized X-ray photoelectron C1s spectra of bare 20-CA (a) and 20-CA loaded with Fe−MEPE at $\mu = 0.10$ (b) and $\mu = 0.16$ (c). (B) X-ray photoelectron C1s difference spectra of 20-CA loaded with Fe−MEPE at $\mu = 0.10$ (a) and $\mu = 0.16$ (b) as well as bulk Fe−MEPE (c), normalized in intensity to spectrum (b). (C) X-ray photoelectron Fe2p$_{3/2}$ spectra of 20-CA loaded with Fe−MEPE (a) $\mu = 0.10$ and (b) $\mu = 0.16$ as well as (c) bulk Fe−MEPE, normalized in intensity to spectrum (b). For details, see text. Spectra in A, B, and C are shifted for clarity.

is a surface-sensitive technique while the other methods are integrating over the whole sample. Specifically, the very high value for CA−MEPE-8 obtained by XPS may indicate that part of the Fe−MEPE was not included in the pores but formed a multilayer film at the outside of the silica grains. Table 3 also shows that the number ratio of nitrogen and Fe atoms has the same value (5.4 ± 0.3) for all composite samples studied by XPS. This indicates that the composition

**TABLE 3: Characterization of the CA−MEPE Samples Specified in Table 2: Fe Content and N/Fe Atomic Ratio**

| | wt % Fe[a] | | | XPS | | |
|---|---|---|---|---|---|---|
| sample | UV−vis | AAS | XPS | at. % Fe | at. % N | N/Fe |
| CA−MEPE-4 | 0.65 | | 0.60 | 0.30 | 1.90 | 5.3 |
| CA−MEPE-5 | 0.83 | 0.93 | | | | |
| CA−MEPE-6 | 1.06 | 0.96 | 1.36 | 0.43 | 2.30 | 5.4 |
| CA−MEPE-7 | 1.27 | 1.14 | | | | |
| CA−MEPE-8 | 1.42 | 1.12 | 1.96 | 0.61 | 3.30 | 5.4 |

[a] wt % Fe of the Fe−MEPE loaded samples as determined by UV−vis, AAS, and XPS.

of Fe−MEPE was the same in these three samples, which is remarkable in view of their very different loadings. For octahedral coordination of the metal centers and infinitely long Fe−MEPE chains, one expects an atom number ratio N/Fe = 6. The somewhat lower experimental value indicates an excess of iron. This result is consistent with the fact that the Fe−MEPE used in these experiments (material I) was prepared with a small metal excess. It thus appears that the stoichiometry of the Fe−MEPE in the pores is similar to that of the original material, in line with the fact that most of the Fe−MEPE is adsorbed in the pores in the high-affinity region of the uptake isotherm.

**3.4. Characterization by Solid-State $^{15}$N NMR.** $^{15}$N solid-state NMR was used to estimate the mean chain length of Fe−MEPE (material II) in bulk and in the pores of 20-CA. This analysis is based on signal deconvolution and observing the change in signal intensities of the Fe-coordinated and free nitrogen atoms ($N_{coor}/N_{free}$) in the ligand molecules before and after uptake of Fe−MEPE in the host material. Because of the relatively low amount of Fe−MEPE in these samples (as compared to the bulk Fe−MEPE materials; cf. Figure 3), it was necessary to use $^{15}$N-labeled material to enhance the $^{15}$N NMR sensitivity. Only the nitrogen atom in the central ring of the ligand was accessible for $^{15}$N labeling, although labeling of the nitrogen atoms in the outer rings would be advantageous because they exhibit a bigger difference in chemical shift between free and coordinated ligand. However, the difference in chemical shift of the central $^{15}$N nuclei between free and coordinated ligand is still sufficient to clearly distinguish these two signals. Figure 9 shows the $^{15}$N MAS NMR and $^{15}$N CPMAS NMR spectra of the $^{15}$N-labeled bulk Fe−MEPE, and the $^{15}$N CPMAS NMR spectrum of a 20-CA−MEPE composite.

The spectrum of $^{15}$N-labeled Fe−MEPE in the bulk state was recorded by $^{15}$N MAS NMR (Figure 9a). This technique directly gives the ratio of coordinated and free nitrogen atoms, $N_{coor}/N_{free}$, from the relative intensities of the corresponding signals. However, this method could not be used for Fe−MEPE embedded in the silica matrix, because of the relatively low concentration of the Fe−MEPE in the samples and the need to use a long recycle delay time (10 min), which would lead to excessive measurement times. Hence, the cross-polarization transfer technique ($^{15}$N CPMAS NMR) was used to study Fe−MEPE both in bulk and embedded in the pores (Figure 9b and c). A disadvantage of this method is that the relative intensities of the peaks in a spectrum may not precisely reflect the relative concentration of the individual species. This problem was reduced by applying a sufficiently long contact time (5 ms) in the pulse sequence. Hence, the relative intensities of the peaks could be mutually compared, and the relative concentrations of the two nitrogen species were estimated from the respective peak intensities of the CPMAS NMR spectra. Assuming that

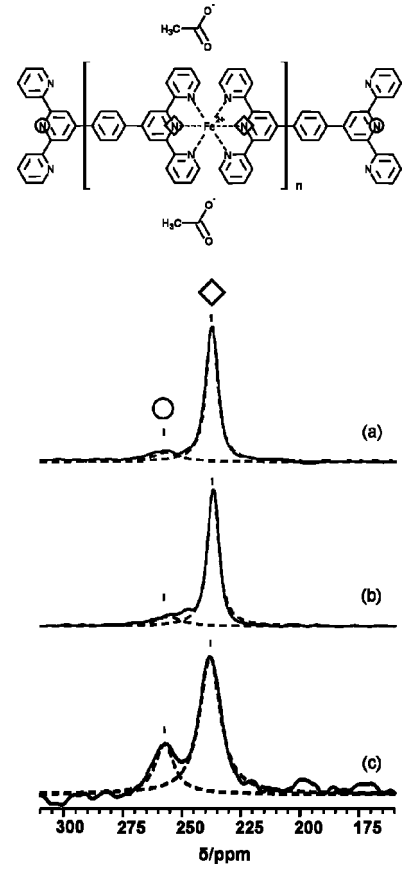


**Figure 9.** (a) $^{15}$N MAS NMR and (b) $^{15}$N CPMAS NMR of bulk solid $^{15}$N Fe−MEPE and (c) $^{15}$N CPMAS NMR of $^{15}$N Fe−MEPE (material II) embedded in the pores of 20-CA silica.

**TABLE 4: Number Ratio of Coordinated and Free $^{15}$N Atoms, $N_{coor}/N_{free}$, and Mean Chain Length, $n$, of Fe−MEPE (Material II) in the Bulk State and in the Pores of 20-CA**

| sample | NMR method | $N_{coor}/N_{free}$ | $n$ |
|---|---|---|---|
| bulk MEPE | MAS | $(15 \pm 1)/2$ | 7−8 |
| bulk MEPE | CP MAS | $(15 \pm 1)/2$ | 7−8 |
| CA−MEPE | CP MAS | $(7 \pm 1)/2$ | 3−4 |

the MEPE chains are terminated on both sides by ligand (as to be expected in the case of ligand excess), then $N_{coor}/N_{free} = 2n/2$, where $n$ is the mean chain length. Results for $N_{coor}/N_{free}$ and $n$ are summarized in Table 4.

For bulk solid Fe−MEPE (Figure 9a and b), signal deconvolution yields $N_{coor}/N_{free} = (15 \pm 1)/2$ for both methods, corresponding to an average chain length $n = 7-8$. The fact that the MAS and CPMAS techniques give concordant results for bulk Fe−MEPE indicates that the CPMAS method may indeed be used for estimating the concentration of the two nitrogen species. On this basis, signal deconvolution of the CPMAS spectrum for Fe−MEPE embedded in silica (Figure 9c) yields $N_{coor}/N_{free} = (7 \pm 1)/2$, corresponding to an average chain length $n = 3-4$. Hence, the results of Table 4 indicate that the mean length of Fe−MEPE chains in the pores of 20-CA is smaller than that in the bulk state. The significant broadening of the signal corresponding to the Fe-coordinated nitrogen species in Figure 9c can be attributed to the confined pore geometry, which reduces the possible orientations of the Fe−MEPE chains inside the pores of CA-20.

**SCHEME 2: Cartoon of the Ion Exchange Transfer of MEPE Polycations (Indicated as $-(-M^{2+}-L-)_n-$) from the Solution into the CA-Functionalized Pores[a]**

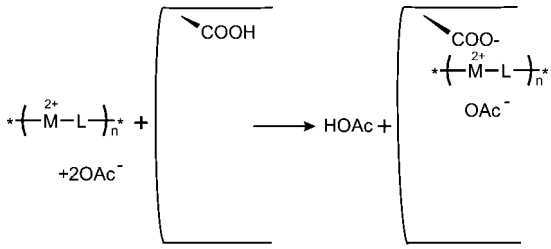


[a] The acetate counterions are partly neutralized by the released protons.

## 4. Discussion

The present study shows that the uptake of Fe−MEPE into the pores of SBA-15 is strongly enhanced when the pore walls are decorated with a layer of CA. This enhancement can be attributed to an ion exchange process and to electrostatic interactions of the Fe−MEPE polycations with the negatively charged pore walls. These two driving forces of the fast uptake process, and the relation between high-affinity adsorption and the arrangement of the MEPE chains in the pores, are discussed below. Finally, the relation between stoichiometry and mean chain length of Fe−MEPE before and after uptake in the pores will be taken up briefly.

**4.1. MEPE Uptake by Ion Exchange.** From the pH change accompanying the initial fast uptake of MEPE from aqueous MEPE, it can be concluded that this process involves an ion exchange in which protons of the silanol or CA groups at the pore walls of the CA−SBA-15 are replaced with Fe−MEPE polycations. In the proposed ion exchange process of Scheme 2, the uptake of a MEPE polycation of $n$ chain segments is accompanied by a release of $n$ protons from undissociated or dissociated carboxylic acid groups at the pore wall. These protons leave the pore space and cause a shift of pH according to the p$K_a$ value of acetic acid. Similarly, in the uptake of MEPE from KOAc solutions, when a fraction $\alpha$ of the carboxylic acid groups at the pore wall exists in deprotonated form, $n\alpha$ potassium ions and $n(1-\alpha)$ protons are released on the uptake of a single polycation of $n$ segments. In either case, the release of a larger number of small ions causes an entropic driving force for the uptake and binding of the polycations in the pore. This offers an explanation for the high rate of the initial uptake. The finding that the ion exchange process with 10-CA causes a larger pH change than with pure SBA-15 (Figure 5) indicates that the CA-doped material has a higher proton donor ability than does pure SBA-15, because the overall proton exchange capacities of the two materials are similar. Tentatively, this higher proton donor ability is attributed to steric effects caused by the flexibility of the propionic acid chains, which allows the COOH groups to get in closer contact with the metal ions of the Fe−MEPE chains than the silanol groups of the surface. The overall proton exchange capacity of 10-CA is estimated as 3.2 mmol/g, about 20% of which are carboxylic acid groups (see Table 1). A simple estimate shows, however, that the number of protons released from the 10-CA matrix during the fast uptake step of Fe−MEPE from a salt-free solution (Figure 5) amounts to only a few percent of the proton exchange capacity of this material (see section S4 in the Supporting Information). Accordingly, the ion exchange mechanism process appears to play only a relatively small role in the uptake of the Fe−MEPE polycations at the weakly acidic pH of the salt-free solution.

**4.2. Effect of Electrostatic Interactions.** Beyond ion exchange, electrostatic interactions will play an important role in the uptake of the Fe−MEPE polycations in the pores. In the aqueous medium, the pore walls of both pure and carboxylic acid-functionalized SBA-15 are negatively charged, but the acid-functionalized silicas have a higher surface charge density than do the pure SBA-15 samples in the pH range of the present study. In particular, whereas the surface charge density of pure silica is only weakly dependent on pH between pH 4 and 8,[41] a more pronounced pH dependence of the surface charge density is found for the carboxylic acid-functionalized SBA-15 materials. This is concluded from FT-IR measurements, which revealed that the ratio of the $COO^-$/COOH peak intensities of 10-CA clearly increases with pH from pH 5.5 ($D_2O$) to pH 8 (phosphate buffer in $D_2O$).[42] On this basis, the difference in MEPE uptake in CA-10 from milli-Q water (pH 5.5) and 0.1 M KOAc (pH 7.25) shown in Figure 6a may be explained by the interplay of two effects: (i) attractive electrostatic interactions between a MEPE polycation and the pore wall; and (ii) repulsive electrostatic interactions between the adsorbed MEPE polycations. Initial adsorption is dominated by the attractive interaction of individual MEPE molecules with the pore wall, which is higher at higher pH due to the higher surface charge density. Electrostatic repulsion between adsorbed MEPE chains becomes significant at higher surface coverage, where it tends to limit the maximum adsorption. However, the range of these repulsive interactions is reduced as the ionic strength of the system is increased by the addition of electrolyte. Accordingly, the repulsive interactions between the adsorbed MEPE chains are expected to be weaker in KOAc than in milli-Q water, leading to a higher adsorption in the presence of KOAc. Hence, both effects are causing a higher adsorption in the presence of KOAc. These conclusions are in line with observations by other authors. Bruzzoniti et al.[43] have found that the retention of Fe(III) ions in CA−SBA-15 increases with increasing pH, and Katiyar et al.[44] observed that the adsorption of a positively charged protein (lysoczyme) in SBA-15 is increased by a factor 2 from pH 5 to 8 in appropriate buffers.

**4.3. Adsorption Affinity and Chain Packing.** The adsorption isotherm of Fe−MEPE in 20-CA (Figure 7) indicates that the high-affinity regime extends to a loading of about 150 mg of Fe−MEPE acetate per 1 g of the matrix. In the study of the uptake kinetics, a similar value was found for the upper limit of the fast-uptake regime. It is of interest to see how this borderline value of the adsorbed amount is related to possible adsorption geometries of the MEPE chains in the pores. The number of adsorbed MEPE units per unit mass of the silica matrix is the respective number for single occupancy of the pores, $\sigma$, multiplied by $S$, the number of chains accommodated side-by-side in each pore.[10] The former number is given by $\sigma = 4v_p/lD^2\pi$, where $v_p$ is the specific pore volume, $D$ is the pore diameter, and $l = 1.5$ nm is the length of a MEPE unit (see Scheme 1). Accordingly, the number of chains arranged side-by-side can be calculated from the experimental data as

$$S = \frac{N_A}{M}\sigma(m_{Fe-MEPE}/m_{silica}) \qquad (2)$$

where $m_{Fe-MEPE}/m_{silica}$ is the mass of Fe−MEPE per unit mass of silica matrix, $M$ is the molar mass of Fe−MEPE, and $N_A$ is Avogadro's constant. The maximum number of MEPE chains, $S_{max}$, that can be accommodated side-by-side in a close-packed monolayer at the pore wall can be estimated from the diameter of the MEPE chain ($d = 1.2$ nm) and the pore diameter $D$. For 20-CA ($D = 8.0$ nm), this yields $S_{max} = 18$. Table 2 indicates

that this value is attained at loadings between sample CA−MEPE-6 and CA−MEPE-7, that is, near the upper limit of the high-affinity adsorption regime of Fe−MEPE in the silica matrix. This supports the conjecture that high-affinity adsorption occurs as long as the Fe−MEPE chains are accommodated in the monolayer in direct contact with the pore wall. Values of $S > 18$, as they are obtained for the samples CA−MEPE-7 and CA−MEPE-8, then indicate the formation of a second layer of Fe−MEPE in the pores or at the outside of the silica grains, or both.

As mentioned earlier, some of the CA−MEPE composite samples of Table 2 were also studied by SAXD. No significant changes in the relative intensities of leading Bragg reflections (10, 11, 20; cf. Figure SI4 in section 3 of the Supporting Information) were observed, as they were found for physisorbed films of vapors at the pore wall of SBA-15.[45,46] However, the MEPE-loaded samples exhibit a significantly lower level of diffuse scattering than does the empty material in the region of higher $q$, so that the 21 Bragg reflection that was masked by diffuse scattering in the empty material is detectable in the material of highest loading with MEPE. Because diffuse scattering is partly due to the roughness of the pore wall, we may conclude that the formation of a layer of MEPE chains reduces the effective roughness of the pore walls. On the other hand, the fact that no significant modulation of the Bragg intensities is observed for the CA−MEPE materials indicates that the layer of MEPE chains is less uniform than a physisorbed fluid film at the pore walls.

**4.4. Stoichiometry and Chain Length of MEPE in the Pores.** Information about the stoichiometry and chain length of Fe−MEPE in the pores was derived from the number ratio of nitrogen and iron atoms (N/Fe) as determined by XPS, and from the number ratio of coordinated and free nitrogen atoms of the ligand ($N_{coor}/N_{free}$) as determined by $^{15}N$ solid-state NMR. The XPS measurements, which were made with Fe−MEPE material I, give the same N/Fe atom ratio for the three CA−MEPE composites studied. This indicates that the stoichiometry of Fe−MEPE in the pores is independent of the degree of loading, which differs strongly for the three samples (Table 3). The experimental atom ratio N/Fe of $5.4 \pm 0.3$ instead of 6 indicates an excess of metal over ligand in the complex, as to be expected for Fe−MEPE material I (see section 2.1). Because the number of segments, $n$, of a chain terminated by metal at both sides ($M_{n+1}L_n$) is related to the atom number ratio as $N/Fe = 6n/(n+1)$, the XPS data indicate a mean chain length $n \approx 9$ or greater for Fe−MEPE material I in the CA−MEPE composite materials. However, this value must be taken with caution, as it relies on the assumption that the MEPE chains are terminated by metal on both ends. Lower values of $n$ would result on the assumption that a fraction of the chains are of type $M_nL_n$ instead of $M_{n+1}L_n$.

The $^{15}N$ MAS NMR measurements were performed with a $^{15}N$-labeled Fe−MEPE (material II) having a ligand excess (see section 2.1), for which one expects that the chains are terminated by ligand on both sides ($M_nL_{n+1}$). From the measured ratio of coordinated and free nitrogen atoms, $N_{coor}/N_{free}$, it was concluded that this Fe−MEPE material has a mean chain length $n = 7-8$ in the bulk state, and a value of about $n = 3-4$ in the pores of 20-CA. Because the measurements were made with the same MEPE material, this result implies that the chains are breaking into two or more fragments when the material is dissolved in the aqueous phase or during the uptake into the pores. For instance, if a MEPE chain $M_nL_{n+1}$ breaks into two fragments:

$$M_nL_{n+1} \rightarrow M_mL_{m+1} + (ML)_{n-m} \quad (3)$$

one of the fragments will not be terminated by ligand on both sides, and thus the relation $N_{coor}/N_{free} = n$ is not strictly applicable for estimating the chain length in the pores. Instead, for the mixture of the fragments, one finds, for any $m < n$, $N_{coor}/N_{free} = (2n-1)/3$, which is smaller than $n$. Hence, the important finding that $N_{coor}/N_{free}$ in the pores is smaller than in the bulk state clearly implies that the MEPE chains are breaking into smaller entities when transferred into the pores. A direct complexation of Fe ions by the surface acid groups might also be envisaged in view of the relatively strong binding of Fe ions to these groups.[43] However, because direct complexation involves a release of ligand L, this alternative seems rather unlikely in view of the high complex formation constants of Fe(II) with the Terpy-type ligands.[47]

## 5. Conclusions

This work has shown that intrinsically stiff metallo-supramolecular polyelectrolytes like Fe−MEPE are adsorbed into the cylindrical nanopores of SBA-15 and that the adsorption affinity is strongly enhanced when the pore walls are functionalized with carboxylic acid groups. Two uptake mechanisms have been identified: a fast process and a slower subsequent process. The fast process is connected with a lowering of pH in the supernatant solution, indicating an ion exchange mechanism. It is favored by increasing the pH, which causes stronger dissociation of the surface functional groups and thus stronger electrostatic interactions of the polycations with the negatively charged pore walls. The nature and rate-determining resistance of the slow process is not fully understood. Generally, an increase of temperature from 20 to 50 °C causes an increase of the adsorption rate and leads to higher levels of adsorption of Fe−MEPE in the pores. For the material 20-CA, in which nearly one-half of the surface silanol is replaced by propionic acid groups, the maximum adsorbed amount corresponds to more than a densely packed layer of Fe−MEPE chains aligned side-by-side along the pores.

Except for the high uptake regime, the results of the uptake measurements by UV−vis analysis of the supernatant are consistent within the error limits with AAS determinations of the iron content in the dry samples. However, XPS measurements gave significantly higher values at high Fe−MEPE loadings. Because XPS is a surface-sensitive probe, this may indicate that at high loadings Fe−MEPE is accumulating near or at the surface of the grains. The metal-to-ligand stoichiometry and average chain length of Fe−MEPE in the matrix were characterized by XPS and $^{15}N$ solid-state NMR spectroscopy. XPS measurements of the atomic ratio of nitrogen to iron showed that the stoichiometry of the Fe−MEPE complex was independent of the level of uptake in the matrix. This result suggests that the Fe−MEPE chains are transferred into the pores as they exist in the solution. $^{15}N$ solid-state NMR measurements of the ratio of coordinated and free nitrogen ($N_{coor}/N_{free}$) were made with a $^{15}N$-labeled Fe−MEPE sample with ligand excess. Assuming that in the Fe−MEPE material obtained under these conditions the chains are terminated by ligand at both ends, the mean chain length was taken as $N_{coor}/N_{free} = n$. For the bulk material, a value $n = 7-8$ was obtained. For the same Fe−MEPE material in the pores of 20-CA, $N_{coor}/N_{free} = n = 3-4$ was found. From the increase of the relative number of free (noncoordinated) nitrogen atoms of the ligand, it was concluded that the Fe−MEPE chains break into smaller entities in the pores, because fragmentation leads to a higher proportion of uncoordinated nitrogen.

**Acknowledgment.** We are indebted to T. Ressler and I. Piotrowski for advice with the AAS measurements. This work was supported by the Deutsche Forschungsgemeinschaft in the framework of SFB 448 "Mesoscopically Organized Composites" and the SONS project "Higher levels of self-assembly of ionic amphiphilic polymers" (FI 235/16-2).

**Supporting Information Available:** Additional figures and explanations to support the material presented in this Article. This material is available free of charge via the Internet at http://pubs.acs.org.

## References and Notes

(1) Zhao, D.; Huo, Q.; Feng, J.; Chmelka, B. F.; Stucky, G. D. *J. Am. Chem. Soc.* **1998**, *120*, 6024.
(2) Kim, D. J.; Dunn, B. C.; Huggins, F.; Huffman, G. P.; Kang, M.; Yie, J. E.; Eyring, E. M. *Energy Fuels* **2006**, *20*, 2608.
(3) Ernst, S.; Glaser, R.; Selle, M. *Prog. Zeolite Microporous Mater.* **1997**, *105*, 1021.
(4) Honma, I.; Sasabe, H.; Zhou, H. S. *Mater. Res. Soc. Symp. Proc.* **1997**, *457*, 525.
(5) Zhu, J.; Kónya, Z.; Puntes, V. F.; Kiricsi, E.; Miao, C. X.; Ager, J. W.; Alivisatos, A. P.; Somorjai, G. A. *Langmuir* **2003**, *19*, 4396.
(6) Holland, B. T.; Walkup, C.; Stein, A. *J. Phys. Chem. B* **1998**, *102*, 4301.
(7) Ganschow, M.; Wark, M.; Wöhrle, D.; Schulz-Ekloff, G. *Angew. Chem.* **2000**, *112*, 167.
(8) Hess, C.; Hoefelmeyer, J. D.; Tilley, T. D. *J. Phys. Chem. B* **2004**, *108*, 9703.
(9) Wang, Y. M.; Wu, Z. Y.; Wang, H. J.; Zhu, J. H. *Adv. Funct. Mater.* **2006**, *16*, 2374.
(10) Akcakayiran, D.; Kurth, D. K.; Röhrs, S.; Rupprechter, G.; Findenegg, G. H. *Langmuir* **2005**, *21*, 7501.
(11) Ernst, S.; Selle, M. *Microporous Mesoporous Mater.* **1999**, *27*, 355.
(12) Zanjanchi, M. A.; Ebrahimian, A.; Alimohammadi, Z. *Opt. Mater.* **2007**, *29*, 794.
(13) Li, D. M.; Zhao, W. J.; Sun, X. D.; Zhang, J. L.; Anpo, M.; Zhao, J. C. *Dyes Pigm.* **2006**, *68*, 33.
(14) Yao, Y. F.; Zhang, M. S.; Shi, J. X.; Gong, M. L.; Zhang, H. J.; Yang, Y. S. *Mater. Lett.* **2001**, *48*, 44.
(15) Ren, T. Z.; Yuan, Z. Y.; Su, B. L. *Colloids Surf., A* **2007**, *300*, 88.
(16) Ren, T. Z.; Yuan, Z. Y.; Su, B. L. *Colloids Surf., A* **2007**, *300*, 79.
(17) Schulz-Ekloff, G.; Wohrle, D.; van Duffel, B.; Schoonheydt, R. A. *Microporous Mesoporous Mater.* **2002**, *51*, 91.
(18) Asefa, T.; MacLachan, M. J.; Coombs, N.; Ozin, G. A. *Nature* **1999**, *402*, 867.
(19) Kurth, D. G.; Lopez, J. P.; Dong, W. F. *Chem. Commun.* **2005**, *16*, 2119.
(20) Han, F. S.; Higuchi, M.; Kurth, D. G. *J. Am. Chem. Soc.* **2000**, *130*, 2073.
(21) Han, F. S.; Higuchi, M.; Kurth, D. G. *Adv. Mater.* **2007**, *19*, 3928.
(22) Bodenthin, Y.; Schwarz, G.; Gutberlet, T.; Geue, T.; Stahn, J.; Möhwald, H.; Kurth, D. G.; Pietsch, U. *Superlattices Microstruct.* **2007**, *41*, 138.
(23) Kurth, D. G.; Higuchi, M. *Soft Matter* **2006**, *2*, 915.
(24) Constable, E. C. *Adv. Inorg. Chem. Radiochem.* **1986**, *30*, 69.
(25) Vermonden, T.; van der Gucht, J.; de Waard, P.; Marcelis, A. T. M.; Besseling, N. A. M.; Sudhölter, E. J. R.; Fleer, G. J.; Cohen Stuart, M. A. *Macromolecules* **2003**, *36*, 7035.
(26) Yang, C.; Wang, Y.; Zibrowius, B.; Schüth, F. *Phys. Chem. Chem. Phys.* **2004**, *6*, 2461.
(27) Kröhnke, F. *Synthesis* **1976**, 1.
(28) Vaduvescu, S.; Potvin, P. G. *Inorg. Chem.* **2002**, *41*, 4081.
(29) Vaduvescu, S.; Potvin, P. G. *Eur. J. Inorg. Chem.* **2004**, 1763.
(30) Morgan, G.; Burstall, F. H. *J. Chem. Soc.* **1937**, 1649.
(31) Sievers, T. K.; Vergin, A.; Möhwald, H.; Kurth, D. G. *Langmuir* **2007**, *23*, 12179.
(32) Hess, C.; Wild, U.; Schlögl, R. *Microporous Mesoporous Mater.* **2006**, *95*, 339.
(33) Briggs, D.; Seah, M. P. *Practical Surface Analysis*; Wiley: Chichester, 1990.
(34) Jaroniec, M.; Solovyov, L. A. *Langmuir* **2006**, *22*, 6757.
(35) Shenderovich, I. G.; Mauder, D.; Akcakayiran, D.; Buntkowsky, G.; Limbach, H.-H.; Findenegg, G. H. *J. Phys. Chem. B* **2007**, *111*, 12088.
(36) Yang, C. M.; Zibrowius, B.; Schmidt, W.; Schüth, F. *Chem. Commun.* **2003**, 1772.
(37) Akcakayiran, D.; Findenegg, G. H.; et al., manuscript in preparation.
(38) Baber, M.; Connor, J. A.; Guest, M. F.; Hillier, I. H.; Schwarz, M.; Stacey, M. *J. Chem. Soc., Faraday Trans. 2* **1973**, *69*, 551.
(39) Maroie, S.; Savy, M.; Verbist, J. *Inorg. Chem.* **1979**, *18*, 2560.
(40) Joseph, Y.; Ketteler, G.; Kuhrs, C.; Ranke, W.; Weiss, W.; Schlögl, R. *Phys. Chem. Chem. Phys.* **2001**, *3*, 4141.
(41) Iler, R. K. *The Chemistry of Silica*; Wiley: New York, 1978.
(42) Akcakayiran, D.; Zebger, I., unpublished results, 2007.
(43) Bruzzoniti, M. C.; Prelle, A.; Sarzanini, C.; Onida, B.; Fiorilli, S.; Garrone, E. *J. Sep. Sci.* **2007**, *30*, 2414.
(44) Katiyar, A.; Ji, L.; Smirniotis, P.; Pinto, N. G. *J. Chromatogr., A* **2005**, *1069*, 119.
(45) Hoffmann, T.; Wallacher, D.; Huber, P.; Birringer, R.; Knorr, K.; Schreiber, A.; Findenegg, G. H. *Phys. Rev. B* **2005**, *72*, 064122.
(46) Zickler, G. A.; Jähnert, S.; Wagermaier, W.; Funari, S. S.; Findenegg, G. H.; Paris, O. *Phys. Rev. B* **2006**, *73*, 184109.
(47) Holyer, R. H.; Hubbard, C. D.; Kettle, S. F.; Wilkins, R. G. *Inorg. Chem.* **1966**, *5*, 622.

JP804712W